

# Transmission Electron Microscopy and Time Resolved Optical Spectroscopy Study of the Electronic and Structural Interactions of ZnO Nanorods with Bovine Serum Albumin

M. Klaumünzer,<sup>†</sup> U. Weichsel,<sup>†</sup> M. Mačković,<sup>‡</sup> E. Spiecker,<sup>‡</sup> W. Peukert,<sup>†</sup> and C. Kryschi<sup>\*,§</sup>

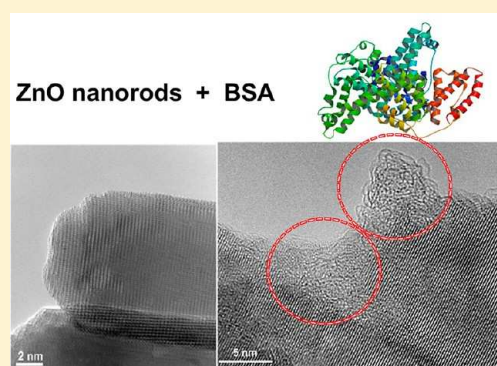
<sup>†</sup>Institute of Particle Technology, Friedrich-Alexander-University Erlangen-Nuremberg, Cauerstr. 4, 91058 Erlangen, Germany

<sup>‡</sup>Center for Nanoanalysis and Electron Microscopy (CENEM), Friedrich-Alexander-University Erlangen-Nuremberg, Cauerstr. 6, 91058 Erlangen, Germany

<sup>§</sup>Department of Chemistry and Pharmacy, Institute of Physical Chemistry I and ICMM, Friedrich-Alexander-University Erlangen-Nuremberg, Egerlandstraße 3, 91058 Erlangen, Germany

## S Supporting Information

**ABSTRACT:** The adsorption behavior and electronic interactions of bovine serum albumin (BSA) with ZnO nanorod surfaces were investigated using high-resolution transmission electron microscopy as well as stationary and time-resolved optical spectroscopy techniques. Transmission electron microscopy shows that ZnO nanorod surfaces are surrounded by a homogeneous amorphous BSA film with thicknesses between  $\sim 2.5$  and  $5.0$  nm. The electronic structure and adsorption geometry of BSA were examined using high-angle annular dark field scanning transmission electron microscopy combined with electron energy loss spectroscopy. The adsorption process was observed to result into an unfolded conformation of BSA becoming predominantly bound in the side-on orientation at the ZnO surface. This adsorption mode of the BSA molecules allows for a strong interaction with surface states of the ZnO nanorods. This is obvious from its efficient quenching of the defect-center photoluminescence of ZnO. Complementary information of electronic interactions across the ZnO nanorod interface was obtained from femtosecond transient absorption spectroscopy experiments. The rise dynamics of the measured transients revealed altered hole trapping dynamics and, thus, indicated to heterogeneous charge transfer as emerging from adsorbed BSA molecules to defect centers of the ZnO interface.



## 1. INTRODUCTION

To date, noble metal and semiconductor nanoparticles with well-defined sizes, shapes, and optical and optoelectronic properties are the focus of intense research activities because of their promising potential for biological and medical applications such as luminescence tagging and imaging, medical diagnostics, drug delivery, and implantable nanoelectronics.<sup>1–4</sup> Nanoparticles may attain biocompatibility and bioactive functions through coating their surfaces with DNA, peptides, and proteins. In particular, for proteins, there have been intense research efforts on the elucidation of their specificity and binding capabilities for noble metal and semiconductor nanoparticles.<sup>3–9</sup> One important issue is that the adsorption process of proteins and their associated nanoparticle-surface mediated conformational changes may provide their complete loss of bioactivity.<sup>10,11</sup> Therefore, engineering of biomedical applications on the basis of protein-conjugated nanoparticles requires fundamental understanding of structural and electronic interactions between proteins and nanoparticle surfaces. Inter alia, it is essential to identify the driving forces and geometry of the protein adsorption process for nanoparticles that were synthesized with a well-defined crystal structure, morphology,

and surface chemistry. Serum albumins play a key role in many physiological functions. They maintain the pH value of blood and are responsible for drug deposition and efficacy. Bovine serum albumin (BSA) has been widely used as model for human serum albumin in biophysical studies.<sup>5,6</sup> BSA is a single polypeptide chain composed of 583 amino acids which are linearly arranged in the tertiary structure in three structurally distinct and evolutionarily related domains (I–III), and each domain consists of two subdomains (A and B).<sup>12</sup> As consisting of various amino acids the BSA polypeptide chain contains three intrinsic fluorophores that are tryptophan, tyrosine, and phenylalanine exhibiting emission in the UV range.<sup>13</sup> At the physiological pH value, the net charges of I, II, and III are  $-11$ ,  $-7$ , and  $+1$ , respectively.<sup>14</sup> This implies that BSA is negatively charged at pH values between 7 and 8. In general, the function and shape of a protein crucially depend on its tertiary structure that may experience significant conformational changes due to adsorption processes at the nanoparticle interfaces. That is why

Received: May 26, 2013

Revised: July 24, 2013

Published: July 26, 2013

the conformational behavior of BSA in conjugation with nanoparticles is of great importance for sensor applications. The simplest way to bind BSA to nanoparticle surfaces is to exploit the electrostatic mechanism. ZnO nanoparticles are an ideal candidate for conjugation with BSA, since this nanomaterial is biocompatible and may be easily prepared with defined sizes and morphologies.<sup>15,16</sup> So far BSA-conjugated ZnO nanoparticles were investigated using the BSA tryptophan fluorescence as probe for electronic interactions.<sup>17–19</sup> Kathiravan and co-workers<sup>17</sup> and Bardhan et al.<sup>18</sup> reported a static quenching mechanism for the BSA fluorescence in the presence of colloidal ZnO nanoparticles. The fluorescence quenching was found to arise from the binding of BSA to ZnO nanoparticles in their electronic ground state. Moreover, these authors could obtain indication of conformational changes of BSA due to interactions with ZnO surfaces. These conformational changes were revealed to result into a somewhat distorted  $\alpha$ -helix of the polypeptide chain and thereupon, into an altered secondary structure of BSA.<sup>18</sup> These preliminary findings show that BSA-conjugated ZnO nanoparticles represent an eligible model system for an in-depth study of conformational and electronic interactions between proteins and semiconductor nanomaterial surfaces.

In this contribution, we examined the electronic and structural interactions between BSA and ZnO nanorod surfaces employing advanced transmission electron microscopy (TEM) techniques and stationary and time-resolved photoluminescence and femtosecond (fs) transient absorption spectroscopy. We are aware that both, morphology and surface structures of ZnO nanoparticles may play essential roles for the adsorption process and conformational reorganization of BSA and, moreover, rule interfacial electron and energy transfer processes. Therefore, our study is based on ZnO nanorods (ZnO NRs) as being producible with definite structural, morphological and optical properties and controllable surface chemistry.<sup>20</sup> As completion to former research work, we probed the static and electronic couplings of BSA to ZnO NR surfaces upon measuring the UV/vis absorption, photoluminescence and fs transient absorption spectra of ZnO NRs coated with BSA.<sup>17–19</sup>

## 2. EXPERIMENTAL SECTION

**2.1. Synthesis of ZnO NRs and Preparation of the BSA Conjugated ZnO NRs.** ZnO NRs were prepared by precipitating zinc acetate dihydrate with potassium hydroxide in methanol and subsequently refluxing for 50 h at 65 °C.<sup>21</sup> ZnO NRs of up to 100 nm in length and 20 nm in diameter were obtained employing this synthesis technique. Lyophilized BSA (Sigma, recrystallized for 5 times; batch no.: 027K0764, EC 232-036-2) was dissolved in Millipore water without further purification. For surface modification of ZnO NRs, the BSA solution was added to the aqueous ZnO NR suspension at the required concentration.

**2.2. Transmission Electron Microscopy.** Conventional transmission electron microscopy (TEM), high-resolution TEM (HRTEM), and scanning TEM (STEM) were performed with a Titan<sup>3</sup> 80-300 (FEI Company, Netherlands) equipped with a Schottky emitter, an image-side Cs-corrector (CEOS), and an energy dispersive X-ray spectroscopy (EDXS) detector, and an imaging electron energy loss spectrometer (EELS, see below). High angle annular dark field scanning TEM (HAADF-STEM) was used to obtain atomic number contrast (Z-contrast) images. TEM images were acquired with a slow scan

charge coupled device (CCD) camera (Gatan, U.S.A.) having an image size of 2048 × 2048 pixels. The analysis of TEM images was carried out using the commercial software DigitalMicrograph (Gatan, USA) and the free available software ImageJ (version 1.45S). All TEM investigations were carried out at 80 kV acceleration voltages. For TEM investigations ZnO/BSA samples were first dispersed in an ethanol/H<sub>2</sub>O solution and then dropped on commonly used TEM copper grids coated with a holey/lacey carbon film.

**2.3. Electron Energy Loss Spectroscopy.** Electron energy loss spectroscopy (EELS) was performed with a Gatan imaging filter (GIF) Tridiem (Gatan, USA). All EEL spectra were acquired in STEM mode, where the sample area contributing to the EEL spectra was defined by the electron probe. The EEL spectra were recorded using 0.2 eV/pixel dispersion, and the energy resolution was 1.2 eV. For every acquired (core-loss) EEL spectrum, the corresponding zero-loss peak (low-loss region of the EEL spectrum) and the plasmon excitations were acquired as well and used for the estimation of the relative sample thickness (in units of the inelastic mean free path of electrons in BSA). The estimation of the relative sample thickness was performed with the commercial software DigitalMicrograph (Gatan, USA), by applying the “log-ratio relative” computing method. For all measurements the relative sample thickness was typically  $\sim 0.3$  that is clearly below one inelastic mean free path of an electron. Hence the multiple scattering events can be neglected, and no deconvolution procedure (correction for multiple-scattering) of the core-loss EEL spectra was needed. All EEL spectra were background-corrected using the power law function as background model. In order to avoid misinterpretation of the EEL spectra, all measurements were accomplished in regions without underlying carbon support film of the TEM grids. No obvious changes in the STEM contrast and/or EEL spectra of the amorphous shells around the ZnO were observed during acquisition, indicating that beam damage is not a severe problem on the time scale of the STEM/EELS analysis.

**2.4. Steady State Absorption and Emission Spectroscopy.** UV/vis absorption spectra were recorded on a Varian Inc. Cary 100 UV/vis spectrophotometer. Photoluminescence (PL) spectra were measured using a FluoroLog 3 spectrofluorometer (Horiba Jobin Yvon GmbH) which is equipped with a double grating on the excitation as well as on the emission side.

**2.5. Femtosecond Transient Absorption Spectroscopy.** The fs transient absorption spectroscopy experiments were conducted with a Clark MXR CPA 2101 laser system in conjunction with an Ultrafast TAPPS HELIOS detection system, consisting primarily of a glass-fiber based spectrometer. The output pulses at 258 nm with a 170 fs pulse and a 1 kHz repetition rate were used as pump pulses. They were obtained by amplifying and frequency-tripling the 775 nm seeding pulses of the Er<sup>3+</sup> doped glass fiber oscillator in a regenerative chirped-pulse titanium-sapphire amplifier and with the frequency doubling BBO crystal, respectively. The samples that are 2 mm quartz cuvettes with aqueous solutions of BSA-conjugated ZnO NRs (1 mg/1 mL) were pumped at pump fluences of ca. 300  $\mu\text{J}/\text{cm}^2$ . Transient absorption spectra were recorded between 400 and 750 nm in the magic-angle configuration with respect to the polarization vectors of pump and probe pulse. The chirp of this spectral range was approximately 350 fs. Transient absorption spectra were obtained as the temporal evolution of the changes in the optical density ( $\Delta\text{OD}$ ) of the

sample. Therefore, a chopper wheel provided the blocking of each second pump pulse so that the probe pulse was alternately transmitted through a pump-pulse excited and a ground-state sample. The intensity of the transmitted probe pulse after the pump-pulse excited sample,  $I^*(\lambda, \tau)$ , and that without pump-pulse excitation,  $I_0(\lambda)$ , were measured as a function of the delay time,  $\tau$ . The  $\Delta OD$  values were determined as  $\Delta OD(\lambda, \tau) = \log[I_0(\lambda)/I^*(\lambda, \tau)]$ .

### 3. RESULTS AND DISCUSSION

**3.1. TEM Studies on BSA Conjugated ZnO NRs.** Figure 1 shows the TEM analysis of ZnO NRs without (a) and with

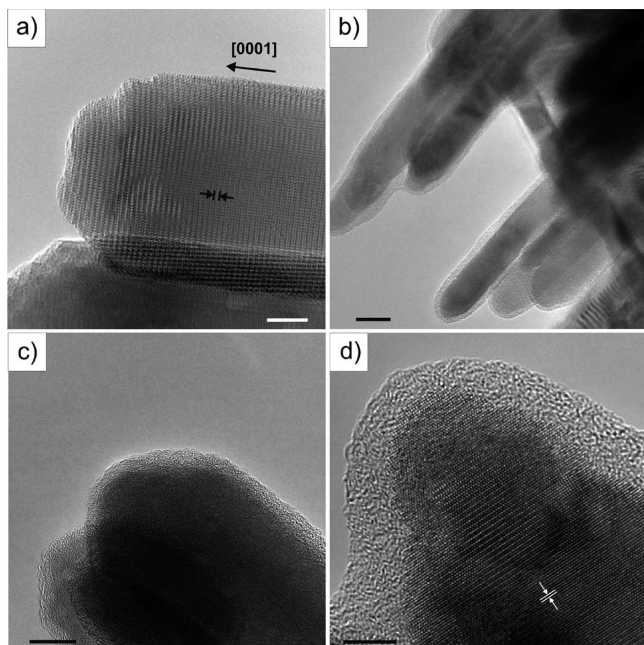


**Figure 1.** TEM analysis of ZnO NRs (a) without and (b–d) with BSA conjugation: HRTEM image in panel a (scale bar = 2 nm) shows two ZnO NRs attached to each other and confirms that no species is present at the interface before BSA conjugation. The interplanar lattice spacing of 0.26 nm corresponds to (0002) lattice planes of the ZnO wurtzite structure. The overview TEM images in panels b (scale bar = 20 nm) and c (scale bar = 10 nm) show ZnO NRs covered with a homogeneous amorphous layer of BSA. The HRTEM image in panel d (scale bar = 5 nm) represents a ZnO NR with BSA adsorbed in the side-on mode.

BSA conjugation (b–d). The HRTEM image in Figure 1a exemplarily shows two ZnO NRs attached to each other along the  $c$ -axis (i.e., (0002) lattice planes with a spacing of 0.26 nm).<sup>22</sup> This image confirms that no species was attached at the ZnO surface, before conjugation with BSA had taken place. The main growth direction of the ZnO NRs is parallel to the [0001] direction which is in good agreement with our former results.<sup>21</sup> Figure 1b–d confirm the successful binding of BSA to the ZnO NR surfaces.

Evidently, the ZnO NR surface is covered with a shell of amorphous material. This shell clearly results from conjugation with BSA, since the corresponding TEM analysis taken from the pristine ZnO NRs (Figure 1a) did not reveal any amorphous material on the surface. The BSA film is homogeneous and has a thickness ranging from 2.5 to 5 nm. The BSA molecules are predominantly adsorbed in the side-on mode onto the ZnO interface.

As being manifested in Figure 2 (see dotted circles), the native BSA conformation was altered during the adsorption

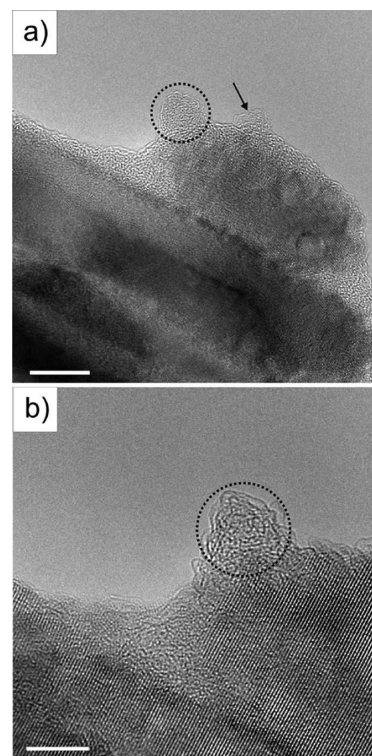


**Figure 2.** HRTEM images of ZnO NRs after conjugation with BSA; in both images (a) (scale bar = 10 nm) and (b) (scale bar = 5 nm) the (0002) lattice planes have an interplanar spacing of 0.26 nm, and BSA is adsorbed in the end-on mode as indicated by black dotted circles and the black arrow.

process to the unfolded and expanded form (Figure 3: F and E form). For a few ZnO NRs the BSA molecules appeared to be adsorbed in the end-on mode as well (Figure 2).

These observed differences in the adsorption behavior of BSA may arise from different surface structures of the ZnO NRs under study.<sup>24</sup> Figure 4a shows a HAADF-STEM image of BSA-conjugated ZnO NRs. The bright contrast in the HAADF-STEM image mainly arises from Zn due to its higher atomic mass number in comparison with BSA as consisting of carbon,

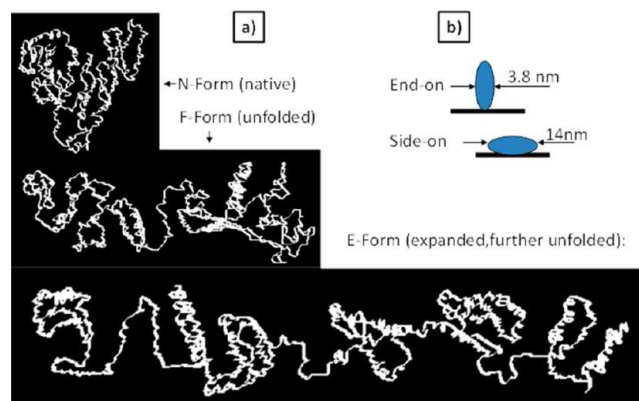


**Figure 3.** Side-on and end-on adsorption modes of BSA at ZnO NR surfaces (a); different conformations of BSA that are the native (N), unfolded (F), and expanded, further unfolded (E) form.<sup>23</sup>

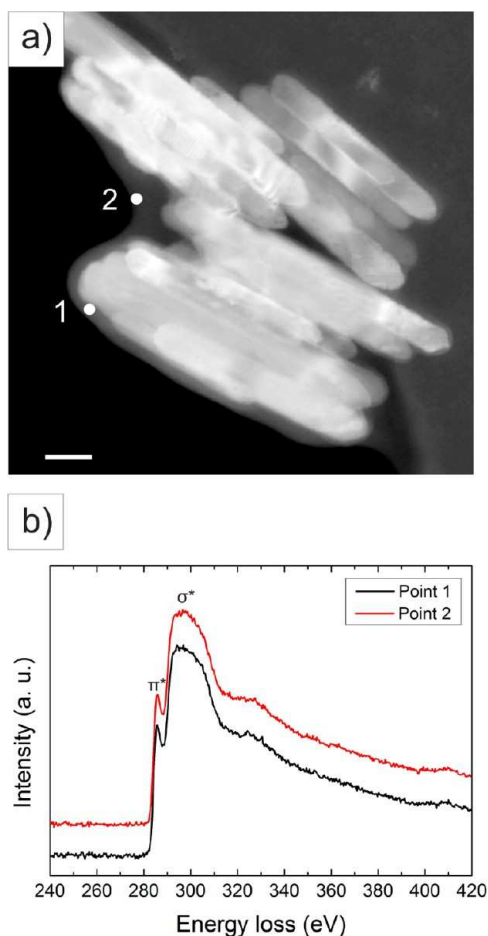


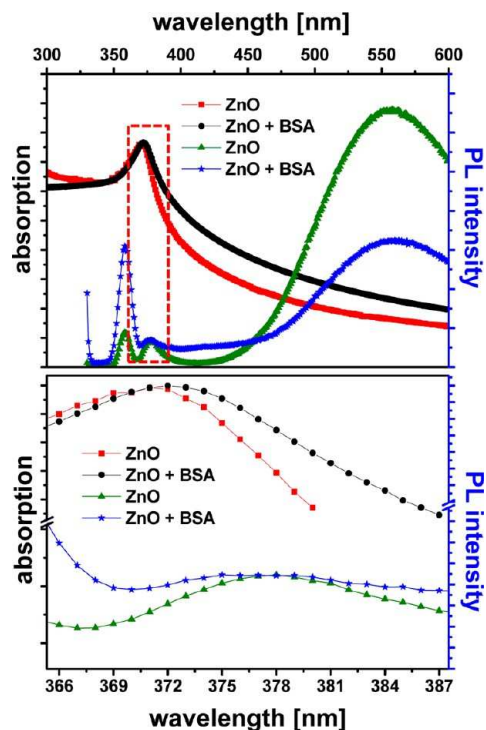
**Figure 4.** HAADF-STEM and EELS analysis of BSA-conjugated ZnO NRs: (a) HAADF-STEM image and (b) EEL spectra at regions marked with white dots (1 and 2) in the HAADF-STEM image.

oxygen, nitrogen, and hydrogen atoms. In order to investigate the local bonding properties of BSA at the ZnO NR surface, STEM-EELS measurements were performed in regions that are marked with white dots in Figure 4a. For the region of BSA at the ZnO NR surface and that of BSA far away from the ZnO NR surface five EEL spectra were recorded, respectively. Figure 4b displays two EEL spectra that are representative for both regions. These EEL spectra show bonding information in terms of the energy-loss near-edge structure (ELNES) of the carbon K-ionization edge.<sup>25,26</sup> The  $\pi^*$  peak is located at an energy loss of 285 eV. This peak stems from transitions to unoccupied antibonding  $\pi^*$  states.

The peak appearing at an energy loss of 293 eV is assigned to transitions to antibonding  $\sigma^*$  states of  $sp^3$ -hybridized carbon. The  $sp^2/sp^3$  peak height ratio was used to evaluate the relative content of  $sp^2$ - and  $sp^3$ -hybridized carbon in BSA. To study the homogeneity of the BSA film, the  $sp^2/sp^3$  peak height ratio of the EEL spectra obtained for the region of BSA at the ZnO NR surface and that of BSA far away from the surface (Figure 4a) was compared with each other. In case of BSA-ZnO interface the  $sp^2/sp^3$  peak height ratio is  $0.639 \pm 0.01$ , whereas that of BSA far away from the ZnO NR surface is  $0.634 \pm 0.02$ . The difference between these two values of the peak height ratio is negligibly small. This implies that ZnO NR surfaces induced conformational changes of BSA which resulted into a homogeneous structure of the BSA film.

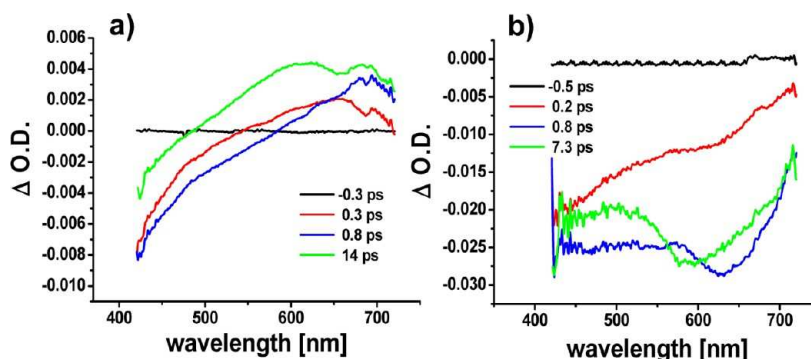
### 3.2. Optical Properties of BSA-Conjugated ZnO NRs.

Figure 5 shows UV/vis absorption and photoluminescence



**Figure 5.** (a) UV/vis absorption spectra (black and red squares) and photoluminescence spectra (blue and green squares) of uncoated ZnO NRs ("ZnO") and BSA-conjugated ZnO NRs ("ZnO + BSA") and (b) the section of the spectra marked by the red-dotted rectangle in panel a is depicted as magnification.

spectra of uncoated ZnO NRs and BSA-conjugated ZnO NRs in water. The photoluminescence (PL) spectra excited at 320 nm (3.87 eV) consist of a Raman water peak at 358 nm (3.46 eV), a prominent PL peak at 372 nm (3.33 eV), and a broad PL band centered at 550 nm. While the UV emission is assigned to radiative recombination of the initially photogenerated electron–hole pairs, the broad PL band in the visible presumably arises from the radiative decay of defect states. These defect states are predominantly located in the surface of the ZnO NRs that are terminated by OH groups, acetate, and water.<sup>21</sup> However, the nature of the responsible defect structures has been still controversially discussed.<sup>15,27–32</sup> The green PL emission around 550 nm is attributed to the radiative recombination of a shallowly trapped electron with a deeply trapped hole.<sup>28</sup> The latter is ascribed to a doubly positively charged oxygen vacancy ( $V_o$ ) that is formed by hole trapping through a monovalent, positively charged oxygen vacancy ( $V_o$ ) at the surface.<sup>15,28,31,32</sup> Since ZnO is an intrinsic n-type semiconductor, there are shallow electron traps that are inherently populated and may provide an electron for radiative recombination, as soon as any hole will be trapped by a  $V_o$  center.<sup>28</sup> Coating of ZnO NRs with BSA obviously results into quenching of the defect-center emission: the PL intensity of the 550-nm band is reduced for 50% when BSA is adsorbed at the surface of the ZnO NRs (Figure 5). This may imply that BSA strongly interacts via its amino acid moieties with surface states of the ZnO. The absorption spectrum displays a small red shift of the band-edge UV absorption for BSA-conjugated ZnO NRs. In contrast, the exciton peak at 372 nm in the PL spectrum



**Figure 6.** Time evolutions of the transient absorption spectra of uncoated ZnO NRs (a) and BSA-conjugated ZnO NRs (b).

does not exhibit any spectral shift. However, the Stokes shift between the absorption and PL spectra of BSA-conjugated ZnO NRs is  $\Delta_{\text{stokes}} = 53$  meV, whereas that of uncoated ZnO NRs is  $\Delta_{\text{stokes}} = 36$  meV (Figure 5b). The significant difference in the Stokes shift of uncoated ZnO NRs and that of BSA-conjugated ZnO NRs is another indication of strong electronic couplings between BSA and ZnO NRs. BSA was reported to form covalent bonds to the ZnO NR surface through hydroxyl groups of its tyrosine moieties.<sup>17</sup> At a pH value of 7 BSA is negatively charged and the surface structures of ZnO nanoparticles, as containing  $\text{Zn}^{2+}$ ,  $\text{Zn}(\text{OH})^+$  ions and positively charged oxygen vacancies, carry predominantly positive charges, which was confirmed by performing Zeta potential measurements on pristine ZnO NRs and BSA-conjugated ZnO NRs (see Supporting Information). Hence BSA may electrostatically interact via its carboxylate anions with the positively charged ZnO NR surface. In particular, electrostatic interactions between carboxylate anions of BSA and monovalent oxygen vacancies in the ZnO surface should impede the formation of doubly positively charged oxygen vacancies and thereupon, are expected to considerably reduce the intensity of the green defect-center PL at 550 nm.

**3.3. Femtosecond Transient Absorption Spectroscopy.** In the femtosecond (fs) transient absorption experiment on ZnO NRs ultrashort (170 fs) pump pulses at 258 nm were used to excite interband transitions and thereupon, create free charge carriers. A temporally delayed white-light continuum probe pulse monitors the absorption of conduction-band electrons and the bleaching of interband absorption transition, while PL emission emerges as an additional contribution to the transmitted white-light continuum probe-pulse intensity. The initially photogenerated free charge carriers may decay via at least three competitive processes that are radiative and radiationless recombination of electron-hole pairs after being relaxed to excitonic states (ca. 60 meV below the conduction band edge) and ultrafast trapping processes into localized states due to lattice or surface defect centers.<sup>27–32</sup> In case of ZnO nanoparticles the conduction-band electrons may be trapped by defect centers such as Zn interstitials or oxygen vacancies which give rise to trap states lying 0.05 eV below the conduction-band edge.<sup>15</sup> However, the population of deep-hole states is expected to rule the rise dynamics of the defect-center PL emission. In fs transient absorption spectra the PL emission increases the transmitted light intensity (e.g., decreases the optical density changes  $\Delta OD$ ), whereas the absorption transitions of conduction band electrons appear as positive values of  $\Delta OD$ .

Transient absorption spectra of uncoated ZnO NRs and BSA-conjugated ZnO NRs dispersed in water were excited at

258 nm and recorded between 400 and 750 nm on a time scale between  $-1.0$  and  $+10$  ps. Figure 6a,b depicts the time evolutions of the transient absorption spectra of uncoated ZnO NRs (a) and BSA-conjugated ZnO NRs (b), respectively. The transient absorption spectra of uncoated ZnO NRs obviously result from a superimposition of blue-green PL emission with photoinduced absorption transitions of the conduction-band electrons which peak at 620 nm. By comparison, BSA-conjugated ZnO NRs exhibit transient absorption spectra that are predominantly composed of contributions due to the blue-green and yellow-red PL emission. The significant differences in the spectral features of uncoated and BSA-conjugated ZnO NRs are understood to follow from efficient electrostatic and electronic interactions between BSA functionalities and ZnO surface states. The lack of the photoinduced absorption band ranging between 500 and 700 nm is explained to originate from ultrafast interfacial transfer of conduction-band electrons to BSA moieties. Interfacial electron transfer does not only significantly deplete the population density of the conduction band and therefore reduces the conduction-band absorption but may also reveal the otherwise superimposed yellow-red PL emission that appears now as prominent minimum between 550 and 700 nm.

Figures 7 and 8 present the kinetic traces detected at the relevant minima or maxima of the transient absorption spectra of uncoated and BSA-conjugated ZnO NRs, respectively. Since the rise dynamics of the kinetic traces are expected to contain information of ultrafast interfacial energy and electron transfer processes, the kinetic traces were calculated using the function

$$S(t) = A(1 - \exp(-t/\tau_{\text{decay}})) + B \exp(-t/\tau_{\text{rise}})$$

where  $\tau_{\text{rise}}$  and  $\tau_{\text{decay}}$  represent the rise time and decay time constant of the kinetic traces, respectively. In case of uncoated ZnO NRs, the best fit of the kinetic trace at 460 nm was obtained with the time constants  $\tau_{\text{rise}} = 0.64$  ps and  $\tau_{\text{decay}} = 2.2$  ps (red solid line in Figure 7b), whereas the calculation of the kinetic traces at 465 and 644 nm yielded for the rise dynamics of both  $\tau_{\text{rise}} = 1.0$  ps and for the decay process  $\tau_{\text{decay}} = 1.25$  ps (465 nm) and  $\tau_{\text{decay}} = 1.4$  ps (644 nm). These results imply that the rise of the kinetic traces becomes significantly prolonged due to the BSA coating. As described in the previous section, the rise dynamics of both blue-green and yellow-red PL are determined by hole trapping through monovalent oxygen vacancies. The slowing-down of the rise dynamics is explained to originate from strong electrostatic interactions between carboxylate anions of BSA and monovalent oxygen vacancies in the ZnO surface. These electrostatic interactions are understood to hamper the hole trapping by oxygen vacancies and

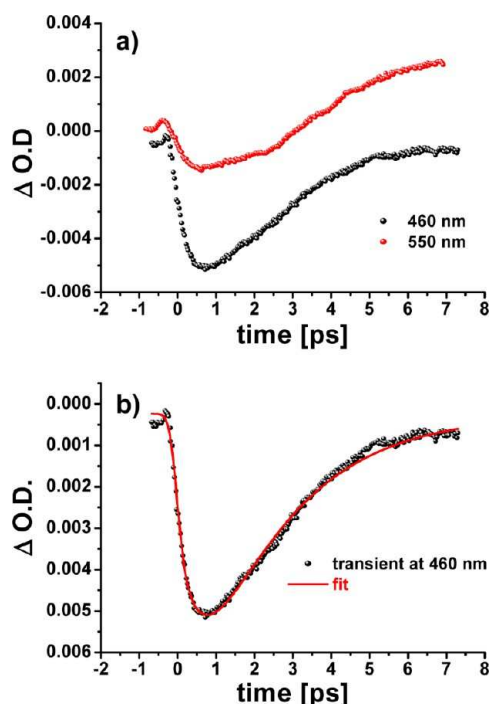


**Figure 7.** (a) Kinetic traces of the transient absorption spectra of uncoated ZnO NRs which were detected at 460 and 550 nm. (b) The kinetic traces detected at 460 nm (black dots) was calculated using the function  $S(t) = 1.0(1 - \exp(-t/2.2 \text{ ps})) + 0.7 \exp(-t/0.64 \text{ ps})$  (red line), where  $\tau_{\text{rise}} = 0.64 \text{ ps}$  and  $\tau_{\text{decay}} = 2.2 \text{ ps}$  are the rise and decay times of the PL signature, respectively.

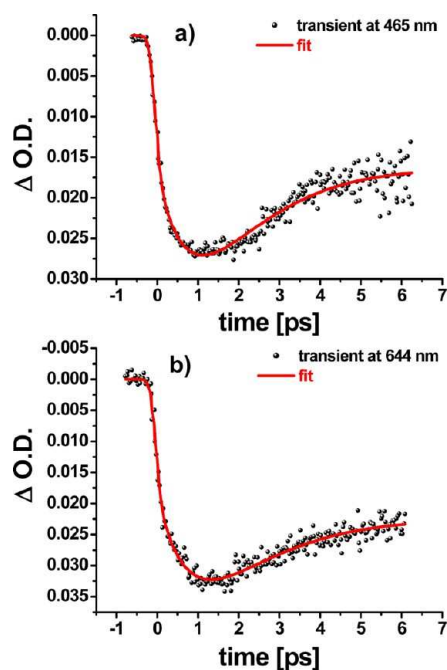


**Figure 8.** Kinetic traces of the transient absorption spectra of BSA-conjugated ZnO NRs detected at 465 nm (a) and 644 nm (b). The respective experimental data (black dots) were calculated using the function  $S(t) = A \exp(-t/\tau_{\text{rise}}) + B(1 - \exp(t/\tau_{\text{decay}}))$  (red line), where the value of  $\tau_{\text{rise}}$  is 1.0 ps and those of  $\tau_{\text{decay}}$  are 1.25 and 1.4 ps, respectively.

thereupon, the radiative recombination of the trapped electron–hole pairs.

## 4. CONCLUSIONS

The structural, morphological, and optical properties of uncoated and BSA-conjugated ZnO NRs were studied using transmission electron microscopy and stationary and ultrafast optical spectroscopy. Adsorption of BSA on ZnO NR surfaces was observed to predominantly take place in the side-on mode and is accompanied by an unfolding and extension process of BSA in the course of forming a homogeneous amorphous film reaching a thickness between  $\sim 2.5$  and  $5.0 \text{ nm}$ . The optical properties of the ZnO NRs, as being manifested in the UV/vis absorption and photoluminescence spectra as well as by the Stokes shift, are significantly affected by structural and electronic interactions with BSA. In particular, the defect-center PL emission is considerably quenched when BSA molecules are adsorbed at the surface. This is explained with the formation of covalent bonds and electrostatic interactions between BSA and the ZnO NR surface. Fs transient absorption spectroscopy experiments on BSA-conjugated and uncoated ZnO NRs were conducted to probe interfacial charge-transfer processes. The transient absorption spectra of uncoated and BSA-conjugated ZnO NRs were observed to appear as a superimposition of blue-green and yellow-red PL emission with absorption transitions of conduction-band electrons. For BSA-conjugated ZnO NRs the yellow-red PL emission predominate the absorption of the conduction-band electrons, which indicates to an ultrafast interfacial transfer of conduction-band electrons to BSA moieties. The rise dynamics of the kinetic traces detected in the spectral ranges of both PL features was found to reflect the formation dynamics of deep hole-trap states due to oxygen vacancies. The rise dynamics of the kinetic traces are significantly slower when BSA is adsorbed at the ZnO NR surface which indicates to efficient interactions between amino moieties of BSA with surface oxygen vacancies of ZnO.

## ■ ASSOCIATED CONTENT

### Supporting Information

Zeta potentials of BSA and ZnO nanorods. This material is available free of charge via the Internet at <http://pubs.acs.org>.

## ■ AUTHOR INFORMATION

### Corresponding Author

\*Fax: +4991318528967. E-mail: [carola.kryschl@fau.de](mailto:carola.kryschl@fau.de).

### Author Contributions

<sup>||</sup>These authors contributed equally.

### Notes

The authors declare no competing financial interest.

## ■ ACKNOWLEDGMENTS

The authors thank the Cluster of Excellence Engineering of Advanced Materials (EAM) and the Deutsche Forschungsgemeinschaft (Research Training Group “Disperse Systems for Electronics” 1161/2) for financial support.

## ■ REFERENCES

- (1) Niemeyer, C. Nanoparticles, Proteins, and Nucleic Acids: Biotechnology Meets Materials Science. *Angew. Chem., Int. Ed.* **2001**, *40*, 4128–4158.
- (2) Katz, E.; Willner, I. Integrated Nanoparticle–Biomolecule Hybrid Systems: Synthesis, Properties, and Applications. *Angew. Chem., Int. Ed.* **2004**, *43*, 6042–6108.

- (3) Agrawal, M.; S. Gupta, S.; Stamm, M. Recent Developments in Fabrication and Applications of Colloid Based Composite Particles. *J. Mater. Chem.* **2011**, *21*, 615–627.
- (4) Aggarwal, P.; Hall, J. B.; McLeland, C. B.; Dobrovolskaia, M. A.; McNeil, S. E. Nanoparticle Interaction with Plasma Proteins as It Relates to Particle Biodistribution, Biocompatibility and Therapeutic Efficacy. *Adv. Drug Delivery Rev.* **2009**, *61*, 428–437.
- (5) Shang, L.; Wang, Y.; Jiang, J.; Dong, S. pH-Dependent Protein Conformational Changes in Albumin: Gold Nanoparticle Bioconjugates: A Spectroscopic Study. *Langmuir* **2007**, *23*, 2714–2721.
- (6) Tantra, R.; Tompkins, J.; Quincey, P. Characterisation of the De-Agglomeration Effects of Bovine Serum Albumin on Nanoparticles in Aqueous Suspension. *Colloids Surf. B* **2010**, *75*, 275–281.
- (7) Sen, T.; Haldar, K.; Patra, A. Au Nanoparticle-Based Surface Energy Transfer Probe for Conformational Changes of BSA Protein. *J. Phys. Chem. C* **2008**, *112*, 17945–17951.
- (8) Mandal, G.; Bardhan, M.; Ganguly, T. Interaction of Bovine Serum Albumin and Albumin-Gold Nanoconjugates with L-Aspartic Acid. A Spectroscopic Approach. *Colloids Surf. B* **2010**, *81*, 178–184.
- (9) Yang, Q.; J. Liang, J.; Han, H. Probing the Interaction of Magnetic Iron Oxide Nanoparticles with Bovine Serum Albumin by Spectroscopic Techniques. *J. Phys. Chem. B* **2009**, *113*, 10454–10458.
- (10) Rana, S.; Yeh, Y.-C.; Rotello, V. M. Engineering the Nanoparticle-Protein Interface: Applications and Possibilities. *Curr. Opin. Chem. Biol.* **2010**, *14*, 828–834.
- (11) Goy-Lopez, S.; Juarez, J.; Alatorre-Meda, M.; Casals, E.; Puentes, V. F.; Taboada, P.; Mosquera, V. Physicochemical Characteristics of Protein–NP Bioconjugates: The Role of Particle Curvature and Solution Conditions on Human Serum Albumin Conformation and Fibrillogenesis Inhibition. *Langmuir* **2012**, *28*, 9113–9126.
- (12) Sogami, M.; Petersen, H. A.; Foster, J. F. Microheterogeneity of Plasma Albumins. V. Permutations in Disulfide Pairings as a Probable Source of Microheterogeneity in Bovine Albumin. *Biochemistry* **1969**, *8*, 49–58.
- (13) Sklar, L. A.; Hudson, B. S.; Simoni, R. D. Conjugated Polyene Fatty Acids as Fluorescent Probes: Binding to Bovine Serum Albumin. *Biochemistry* **1977**, *16*, 5100–5108.
- (14) Togashi, D. M.; Ryder, A. G.; McMahon, D.; Dunne, P.; McManus, J. Fluorescence Study of Bovine Serum Albumin and Ti and Sn Oxide Nanoparticles Interactions. *SPIE-OSA* **2007**, *6628*, 66281K.
- (15) Djurišić, A. B.; Hang Leung, Y. Optical Properties of ZnO Nanostructures. *Small* **2006**, *2*, 944–961.
- (16) Kim, K.-M.; Kim, T.-H.; Kim, H.-M.; Kim, H.-J.; Gwak, G.-H.; Paek, S.-M.; Oh, J.-M. Colloidal Behaviors of ZnO Nanoparticles in Various Aqueous Media. *Toxicol. Environ. Health. Sci.* **2012**, *4*, 121–131.
- (17) Kathiravan, A.; Paramaguru, G.; Renganathan, R. Study on the Binding of Colloidal Zinc Oxide Nanoparticles with Bovine Serum Albumin. *J. Mol. Struct.* **2009**, *934*, 129–137.
- (18) Bardhan, M.; Mandal, G.; Ganguly, T. Steady State, Time Resolved, and Circular Dichroism Spectroscopic Studies to Reveal the Nature of Interactions of Zinc Oxide Nanoparticles with Transport Protein Bovine Serum Albumin and to Monitor the Possible Protein Conformational Changes. *J. Appl. Phys.* **2009**, *106*, 034701.
- (19) Tantra, R.; Tompkins, J.; Quincey, P. Characterisation of the De-Agglomeration Effects of Bovine Serum Albumin on Nanoparticles in Aqueous Suspension. *Colloids Surf. B* **2010**, *75*, 275–281.
- (20) Voigt, M.; Klaumünzer, M.; Ebel, A.; Werner, F.; Yang, G.; Marczak, R.; Spiecker, E.; Guldi, D. M.; Hirsch, A.; Peukert, W. Surface Functionalization of ZnO Nanorods with C60 Derivatives Carrying Phosphonic Acid Functionalities. *J. Phys. Chem. C* **2011**, *115*, 5561–5565.
- (21) Voigt, M.; Klaumünzer, M.; Thiem, H.; Peukert, W. Detailed Analysis of the Growth Kinetics of ZnO Nanorods in Methanol. *J. Phys. Chem. C* **2010**, *114*, 6243–6249.
- (22) Huang, M. H.; Mao, S.; Feick, H.; Yan, H.; Wu, Y.; Kind, H.; Weber, E.; Russo, R.; Wang, P. Room-Temperature Ultraviolet Nanowire Nanolasers. *Science* **2001**, *292*, 1897–1899.
- (23) Sun, C.; Yang, J.; Wu, X.; Huang, X.; Wang, F.; Liu, S. Unfolding and Refolding of Bovine Serum Albumin Induced by Cetylpyridinium Bromide. *Biophys. J.* **2005**, *88*, 3518–3524.
- (24) Peters, T., Jr. Atomic Structure and Chemistry of Human Serum Albumin. *Adv. Protein Chem.* **1985**, *37*, 161–245.
- (25) Garvie, L. A. J.; Craven, A. J.; Brydson, R. Use of Electron-Energy Loss Near-Edge Fine Structure in the Study of Minerals. *Am. Mineral.* **1994**, *79*, 411–425.
- (26) Wronski, Z. S.; Carpenter, G. J. C. Carbon Nanoshells Obtained from Leaching Carbonyl Nickel Metal Powders. *Carbon* **2006**, *44*, 1779–1789.
- (27) Liu, Z. W.; Ong, C. K.; Yu, T.; Shen, Z. X. Catalyst-Free Pulsed-Laser-Deposited ZnO Nanorods and Their Room-Temperature Photoluminescence Properties. *Appl. Phys. Lett.* **2006**, *88*, 053110.
- (28) Bauer, C.; Boschloo, G.; Mukhtar, E.; Hagfeldt, A. Ultrafast Relaxation Dynamics of Charge Carriers Relaxation in ZnO Nanocrystalline Thin Films. *Chem. Phys. Lett.* **2004**, *387*, 176–181.
- (29) House, R. L.; Mehl, B. P.; Kirschbrown, J. R.; Barnes, S. C.; Papanikolas, J. M. Characterizing the Ultrafast Charge Carrier Trapping Dynamics in Single ZnO Rods Using Two-Photon Emission Microscopy. *J. Phys. Chem. C* **2011**, *115*, 10806–10816.
- (30) Zhou, X.; Kuang, Q.; Jiang, Z.-Y.; Xie, Z.-X.; Xu, T.; Huang, R.-B.; Zheng, L.-S. *J. Phys. Chem. C* **2007**, *111*, 12091–12093.
- (31) Woo Lee, W.; Been Kim, S.; Yi, J.; Nichols, W. T.; Il Park, W. The Origin of Green Emission of ZnO Microcrystallites: Surface-Dependent Light Emission Studied by Cathodoluminescence. *J. Phys. Chem. C* **2011**, *116*, 456–460.
- (32) van Dijken, A.; Meulenkaamp, E. A.; Vanmaekelbergh, D.; Meijerink, A. The Kinetics of the Radiative and Nonradiative Processes in Nanocrystalline ZnO Particles upon Photoexcitation. *J. Phys. Chem. B* **2000**, *104*, 1715–1723.